Inorg. Chem. **2007**, *46*, 9743–9753

Synthesis, Structural, and Magnetic Studies on a Redox Family of Tetrametallic Vanadium Clusters: $\{V^{IV}_4\}$, $\{V^{III}_2V^{IV}_2\}$, and $\{V^{III}_4\}$ Butterfly Complexes

Ian S. Tidmarsh,[†] Emma Scales,[†] Paul R. Brearley,[†] Joanna Wolowska,[‡] Lorenzo Sorace,*[,§] Andrea Caneschi,[§] Rebecca H. Laye,*[,†] and Eric J. L. McInnes*[,†]

School of Chemistry, The University of Manchester, Manchester M13 9PL, U.K; EPSRC c.w. EPR Service Centre, School of Chemistry, The University of Manchester, Manchester M13 9PL, U.K; Dipartimento di Chimica, Università di Firenze, and UdR INSTM, Via della Lastruccia 3, Sesto Fiorentino, Italy

Received June 7, 2007

The synthesis, crystal structures, and magnetic properties are reported for a redox family of butterfly-type tetrametallic vanadium alkoxide clusters, namely $[V_2(VO)_2(acac)_4(RC\{CH_2O\}_3)_2]$ (R = Me **1**, Et **2**, CH_2OH **3**), $[V_2(VO)_2(acac)_2(O_2CPh)_2(MeC\{CH_2O\}_3)_2]$ (**5**), $[(VO)_4(MeOH)_2(O_2CPh)_2(\{HOCH_2\}C\{CH_2O\}_3)_2]$ (**6**), $[V_4Cl_2(dbm)_4(RC\{CH_2OH\}_3)_2]$ (R = Me **7**, Et **8**, CH_2OH **9**), and $[V_4Cl_2(dbm)_4(MeO)_6]$ (**10**). The cluster cores are $\{V^{IV}_4\}$ (**6**), $\{V^{III}_2V^{IV}_2\}$ (**1**–**5**), and $\{V^{III}_4\}$ (**7**–**10**), with examples of both isomeric forms of the of the mixed-valence cores (either V^{III} or V^{IV} ions forming the butterfly body). Magnetic studies reveal the clusters to be dominated by antiferromagnetic exchange interactions in each case. The magnetic exchange parameters are determined for representative examples of each core type. $\{V^{IV}_4\}$ and $\{V^{III}_4\}$ have diamagnetic ground states. The two isomeric $\{V^{III}_2V^{IV}_2\}$ types are found to give rise to either an $S = 0$ ground state with a number of low-lying excited states due to competing antiferromagnetic exchange interactions (V^{III}_2 butterfly body) or to a well-isolated $S = 1$ ground state (V^{IV}_2 butterfly body).

Introduction

Vanadium-cluster chemistry has extraordinary flexibility due to the range of available metal oxidation states and coordination geometries. However, the literature is dominated by the high-valent, $V^{IV/V}$ chemistry − the important polyoxovanadates and related species.[1] Recently, we have been exploring the cluster chemistry of lower-valent states in an attempt to prepare interesting magnetic clusters based on the V^{III} ion. This d^2, $S = 1$ ion typically exhibits a large zero-field splitting (ZFS)[2] and, hence, is attractive as a building block toward magnetic materials such as single-molecule magnets. Indeed, Christou has reported a $\{V^{III}_4\}$ cluster that exhibits SMM behavior.[3] However, there are very few low-valent V^{III} or $V^{III/IV}$ clusters in the literature[4,5] due to the reducing nature of V^{III} and the inherent stability of the $\{V^{IV}O\}^{2+}$ vanadyl and $\{V^{V}O\}^{3+}$ ions. We have been successful in preparing several large homovalent V^{III} [6] and heterovalent $V^{III/IV}$ [7] clusters by exploiting solvothermal synthetic methods in alcohols, with nuclearities of up to 10 for the former[6a] and 18 for the latter ($V^{III}_{16}V^{IV}_2$)[7b]. However, whereas there are a few important magnetic studies on small

* To whom correspondence should be addressed. E-mail: eric.mcinnes@manchester.ac.uk.
[†] School of Chemistry, The University of Manchester.
[‡] EPSRC c.w. EPR Service Centre, School of Chemistry, The University of Manchester.
[§] Dipartimento di Chimica, Università di Firenze, and UdR INSTM.

(1) For example, see: (a) Pope, M. T.; Müller, A. *Angew. Chem., Int. Ed.* **1991**, *30*, 34. (b) Chen, Q.; Zubieta, J. *Coord. Chem. Rev.* **1992**, *114*, 107. (c) Zubieta, J. *Mol. Eng.* **1993**, *3*, 93. (d) Khan, M. I.; Zubieta, J. *Prog. Inorg. Chem.* **1995**, *43*, 1.
(2) (a) Tregenna-Piggott, P. L. W.; Weihe, H.; Bendix, J.; Barra, A.-L.; Güdel, H. U. *Inorg. Chem.* **1999**, *38*, 5928. (b) Krzystek, J.; Fiedler, A. T.; Sokol, J.; Ozarowski, A.; Zvyagin, S. A.; Brunold, T. C.; Long, J. R.; Brunel, L-C.; Telser, J. *Inorg. Chem.* **2004**, *43*, 4654.
(3) Castro, S. L.; Sun, Z.; Grant, C. M.; Bollinger, J. C.; Hendrickson D. N.; Christou, G. *J. Am. Chem. Soc*. **1998**, *120*, 2365.
(4) (a) Lee, I. S.; Long, J. R. *Chem. Commun*. **2004**, 3234. (b) Fry, F. H.; Dougan, B. A.; McCann, N.; Ziegler, C.; Brasch, N. E. *Inorg. Chem*. **2005**, *44*, 5197. (c) Kumagai, H.; Kitagawa, S. *Chem. Lett*. **1996**, 471. (d) Salta, J.; Zubieta, J. *J. Cluster Sci.* **1996**, *7*, 531.
(5) Mikuriya, M.; Kotera, T.; Adachi F.; Bandow, S. *Chem. Lett*. **1993**, 945.
(6) (a) Laye, R. H.; Murrie, M.; Ochsenbein, S.; Bell, A. R.; Teat, S.; Raftery, J.; Güdel, H. U.; McInnes, E. J. L. *Chem. Eur. J*. **2003**, *9*, 6215. (b) Laye, R. H.; Larsen, F. K.; Overgaard, J.; Muryn, C. A.; McInnes, E. J. L.; Rentschler, E.; Sanchez, V.; Teat, S. J.; Güdel, H. U.; Waldmann, O.; Timco, G. A.; Winpenny, R. E. P. *Chem. Commun*. **2005**, 1125.

10.1021/ic7011183 CCC: $37.00
Published on Web 10/05/2007

Scheme 1[a]

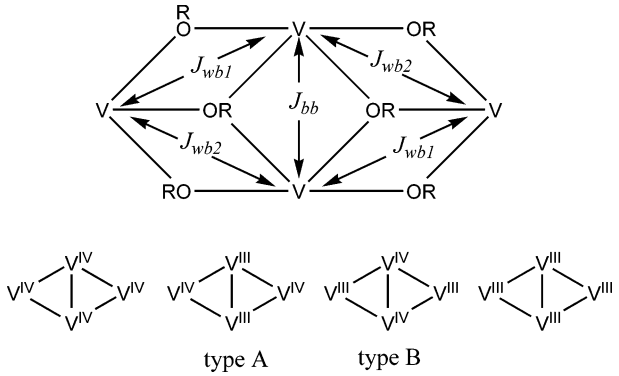

[a] Top: Representation of a $\{V_4\}$ butterfly-type vanadium alkoxide core (top), showing possible magnetic exchange interactions between the body (J_{bb}) and between the body and wingtip (J_{wb1} and J_{wb2}; $J_{wb1} = J_{wb2}$ for a regular rhombus) metal ions. Bottom: Metal oxidation states in the cores of **1**−**10** reported in this work.

V^{IV} clusters,[8,9] which give insight into larger systems, interpretation of the magnetic data of large V^{III} or $V^{III/IV}$ species is hampered by the lack of data for smaller examples. There are some important studies, including Christou's tetramer,[3] Wieghardt's remarkably strongly ferromagnetically coupled V^{III} dimer,[10] and a theoretical study on $V^{III}-O-V^{III}$ coupling by Weihe and Güdel.[11] However, well-studied examples larger than dimers[12] are rare.

Mikuriya's[5] $\{V^{III}_2V^{IV}_2\}$ cluster $[V_2(VO)_2(acac)_4(OMe)_6]$ was intriguing to this end because as well as being the only $V^{III/IV}$ tetrametallic cluster reported to date, it is based on the well-known butterfly structural motif (Scheme 1). Related $\{V^{V}_4\}$ and $\{V^{IV}_4\}$ alkoxide-bridged butterfly complexes have been reported: Crans and co-workers' $[(VO)_4(MeC\{CH_2O\}_3)_2(OMe)_6]$[13] and Plass' $[(VO)_4(acac)_2(Htea)_2(OMe)_2]$[14] and $[(VO)_4(acac)_2(L)_2(OMe)_2]$[15] [$MeC\{CH_2OH\}_3$ = tris-(hydroxymethyl)ethane; H_3tea = triethanolamine; H_2L = *N*,*N*-*bis*(2-hydroxyethyl)-*N*′-(2-pyrrolyl-methylidene)ethylenediamine]. These clusters imply that this butterfly cluster core, bridged by alkoxides, can stabilize a range of oxidation states. Zubieta[1d] and Müller[16] have noted the ability of alkoxides to stabilize fully reduced, all-V^{IV}, polyoxo(alkoxo)vanadates by reducing charge density cf. naked polyoxovanadates. Given our success with stabilizing large V^{III} and $V^{III/IV}$ clusters by solvothermal synthesis in alcohols, we reasoned that we should be able to extend the vanadium butterfly family to include $\{V^{III}_4\}$ and other $\{V^{III}_2V^{IV}_2\}$ species.

Mikuriya's complex was prepared by the reduction of $[VO(acac)_2]$ with a thiolate in $MeOH/CH_2Cl_2$ (the yield was not reported).[5] In this work, we report a much-more facile synthesis, via a solvothermal route and in excellent yields, of four new $\{V^{III}_2V^{IV}_2\}$ clusters. These have analogous alkoxide-bridged butterfly cores, and, moreover, provide examples where the butterfly bodies are V^{III} (*type A*, Scheme 1; as in Mikuriya's compound) *and* the previously unknown isomeric core, where the V^{IV} ions form the butterfly body (*type B*, Scheme 1). Furthermore, we report the synthesis of four examples of the all-V^{III} analogues of this core − formally by the substitution of $\{V^{IV}{=}O\}^{2+}$ with the isoelectronic fragment $\{V^{III}-Cl\}^{2+}$ − again by solvothermal methods and in excellent yields. We also report a new example of the all-V^{IV} core. Hence, these complexes represent a unique redox family of compounds. Magnetic studies are presented for examples of the $\{V^{IV}_4\}$, both forms of the $\{V^{III}_2V^{IV}_2\}$ and the $\{V^{III}_4\}$ species, allowing the comparison of the magnetic exchange coupling constants and consequent electronic structure throughout the family.

Experimental Section

Physical Measurements. IR data was measured on KBr pellets on a PerkinElmer FTIR spectrometer. MS measurements were conducted on either a VG Trio 2000 (electrospray) or on a Waters Micro mass TofSpec 2E (MALDI) spectrometer. EPR data were collected on ESP-300 (Q-band) and Elexsys E600 (W band) spectrometers. Variable-temperature magnetic data were measured with a Cryogenic S600 SQUID magnetometer on polycrystalline samples in 1 (300−35 K) and 0.1 (<35 K) T field. Low temperature (1.5 K), variable-field (up to 12 T) magnetization measurements were measured on an Oxford Instruments vibrating-sample magnetometer. The data were corrected for the contribution of the sample holder and for the diamagnetism of the sample estimated from Pascal's constants. Modeling of magnetic susceptibility data was performed by matrix diagonalization methods using *CLUMAG*[17] software.

X-ray Diffraction. Single-crystal X-ray diffraction data were measured on an Oxford Diffraction XCalibur2 diffractometer with the exception of **6** and **9**, which were measured on a Bruker SMARTAPEX CCD diffractometer. Structural solution and refinement were performed with *SHELXTL*.[18] Structures were solved by direct methods. Refinement of F^2 was against all reflections. All of the non-hydrogen atoms were refined anisotropically except for the disordered MeCN molecule in the lattice of **9** [N(2) C(39) C(38)], in which N(2) and C(38) share the same atomic coordinates. This molecule also required the application of geometrical and displacement restraints. It was also necessary to use geometrical and displacement restraints in the refinement of **7** to deal with the THF solvent molecule [O(8) C(36) C(37) C(38) C(39)], which is disordered over two sites. A similar treatment was required to model the disordered hydroxyl group [O(8)] of the

(7) (a) Laye, R. H.; Wei, Q.; Mason, P. V.; Shanmugan, M.; Teat, S. J.; Brechin, E. K.; Collison, D.; McInnes, E. J. L. *J. Am. Chem. Soc.* **2006**, *128*, 9020. (b) Tidmarsh, I. S.; Laye, R. H.; Brearley, P. R.; Shanmugan, M.; Sañudo, E. C.; Sorace, L.; Caneschi, A.; McInnes, E. J. L. *Chem. Commun.* **2006**, 2560. (c) Shaw, R.; Laye, R. H.; Jones, L. F.; Low, D. M.; Talbot-Eeckelaers, C.; Wei, Q.; Milios, C. J.; Teat, S.; Helliwell, M.; Raftery, J.; Evangelisti, M.; Affronte, M.; Collison, D.; Brechin, E. K.; McInnes, E. J. L. *Inorg. Chem.* **2007**, *46*, 4968. (d) Tidmarsh, I. S.; Laye, R. H.; Brearley, P.R.; Shanmugam, M.; Sañudo, E. C.; Sorace, L.; Caneschi, A.; McInnes, E. J. L. *Chem.*−*Eur. J.* **2007**, *13*, 6329.
(8) Plass, W. *Angew. Chem., Int. Ed. Engl.* **1996**, *35*, 627.
(9) Hegetschweiler, K.; Morgenstern, B.; Zubieta, J.; Hagrman, P. J.; Lima, N.; Sessoli R.; Totti, F. *Angew. Chem., Int. Ed.* **2004**, *43*, 3436.
(10) Knopp, P.; Wieghardt, K.; Nuber, B.; Weiss, J.; Sheldrick, W.S. *Inorg. Chem.* **1990**, *29*, 363.
(11) Weihe, H.; Güdel, H. U. *J. Am. Chem. Soc.* **1998**, *120*, 2870.
(12) Kanamori, K.; *Coord. Chem. Rev.* **2003**, *237*, 147, and references therein.
(13) Crans, D. C.; Jiang, F.; Chen, J.; Anderson, O. P.; Miller, M. M. *Inorg. Chem.* **1997**, *36*, 1038.
(14) Plass, W. *Eur. J. Inorg. Chem.* **1998**, 799.
(15) Plass, W. *Inorg. Chem.* **1997**, *36*, 2200.
(16) Müller, A.; Meyer, J.; Bogge, H.; Stammler, A.; Botar, A. *Chem.*−*Eur. J.* **1998**, *4*, 1388.
(17) Gatteschi, D.; Pardi, L. *Gazz. Chim. Ital.* **1993**, *123*, 231.
(18) *SHELX-PC Package*, Bruker Analytical X-ray Systems: Madison, WI, 1998.

Table 1. Unit-Cell Details of **1**−**5**

	1	**2**	**3**	**4**	**5**
formula	$C_{32}H_{49}O_{16}NV_4$	$C_{32}H_{50}O_{16}V_4$	$C_{30}H_{46}O_{18}V_4$	$C_{30}H_{46}O_{16}V_4$	$C_{30}H_{46}O_{18}V_4$
fw	907.48	894.48	898.43	866.43	938.49
cryst dimensions (mm)	0.39 × 0.28 × 0.15	0.41 × 0.30 × 0.21	0.44 × 0.41 × 0.40	0.54 × 0.41 × 0.26	0.41 × 0.34 × 0.24
cryst syst	monoclinic	orthorhombic	orthorhombic	monoclinic	monoclinic
space group	*C*2/*c*	*Pbca*	*Pbca*	*P*2(1)/*n*	*P*2(1)/*n*
a (Å)	23.992(3)	16.4089(6)	15.6887(16)	10.2091(4)	9.2831(3)
b (Å)	11.0699(6)	14.1745(5)	13.5545(14)	15.6663(7)	11.1266(4)
c (Å)	16.632(2)	16.5690(5)	17.3368(19)	11.3058(5)	19.4966(7)
α (deg)	90	90	90	90	90
β (deg)	117.814(3)	90	90	91.770(3)	102.773(3)
γ (deg)	90	90	90	90	90
U (Å^3)	3907.1(7)	3853.7(2)	3686.7(7)	1807.37(13)	1963.96(12)
Z	4	4	4	2	2
ρ_{calcd}	1.543	1.542	1.619	1.592	1.587
T (K)	100(2)	100(2)	100(2)	100(2)	100(2)
$2\theta_{max}$	63.74	63.97	64.06	63.79	63.51
data collected (unique)	12 238 (3284)	37 290 (5862)	22 957 (3096)	17 947 (5480)	5126 (2562)
Data used [$I > 2\sigma(I)$]	2190	4219	1942	4265	2282
no. of params	246	240	240	231	256
R(*F*)	0.0446	0.0357	0.0504	0.0283	0.0356
wR2	0.1090	0.0978	0.1093	0.0763	0.0976
$\Delta\rho_{min}$ (eÅ^{-3})	−0.862	−0.468	−0.481	−0.446	−0.516
$\Delta\rho_{max}$ (eÅ^{-3})	0.505	0.890	0.688	0.762	0.393

Table 2. Unit-Cell Details of **6**−**10**

	6	**7**	**8**	**9**	**10**
formula	$C_{30}H_{52}O_{22}V_4$	$C_{74}H_{70}O_{15}Cl_2V_4$	$C_{72}H_{66}O_{14}Cl_2V_4$	$C_{72.5}H_{67}O_{16.5}N_1Cl_2V_4$	$C_{66}H_{62}O_{14}Cl_2V_4$
fw	968.48	1473.96	1429.91	1490.93	1353.82
cryst dimensions (mm)	0.35 × 0.30 × 0.15	0.43 × 0.27 × 0.05	0.44 × 0.32 × 0.20	0.50 × 0.25 × 0.20	0.36 × 0.21 × 0.19
cryst syst	triclinic	monoclinic	triclinic	tetragonal	monoclinic
space group	$P\bar{1}$	*C*2/*c*	$P\bar{1}$	*I*4(1)/*a*	*P*2(1)/*c*
a (Å)	11.067(8)	24.473(6)	11.1495(4)	28.1794(14)	10.7183(16)
b (Å)	12.034(9)	11.0449(15)	13.4573(4)	28.1794(14)	25.3971(18)
c (Å)	17.256(13)	25.0270(3)	22.8482(8)	17.0456(12)	11.8682(11)
α (deg)	102.367(14)	90	78.970(3)	90	90
β (deg)	94.480(13)	104.667(13)	89.538(3)	90	108.142(11)
γ (deg)	114.203(12)	90	68.743(3)	90	90
U (Å^3)	2012(3)	6544(2)	3128.88(18)	13535.5(13)	3070.1(6)
Z	2	4	2	8	2
ρ_{calcd}	1.599	1.496	1.518	1.463	1.464
T (K)	100(2)	100(2)	100(2)	100(2)	100(2)
$2\theta_{max}$	56.4	63.80	63.79	54.16	56.32
data collected (unique)	12 398 (8804)	21 436 (6657)	23 547 (12684)	38 660 (6941)	21 984 (6263)
data used [$I > 2\sigma(I)$]	6891	5127	10 377	4954	4256
no. of params	516	448	831	466	391
R(*F*)	0.0618	0.0834	0.0427	0.0374	0.0326
wR2	0.1681	0.1741	0.1172	0.0991	0.0795
$\Delta\rho_{min}$ (eÅ^{-3})	−1.056	−0.880	−0.836	−0.238	−0.410
$\Delta\rho_{max}$ (eÅ^{-3})	1.021	0.714	1.032	0.774	0.379

($\{HOCH_2\}C\{CH_2O\}_3)^{3-}$ ligand of **9**, which is disordered over three sites. Hydrogen atoms were added in geometrically calculated positions. Crystal details are summarized in Tables 1 and 2.

Synthesis. All of the chemicals were purchased from Aldrich, except for $[VO(acac)_2]$, which was purchased from Lancaster, and were used without further purification. $[VCl_3(THF)_3]$, $[V_3(O)(PhCO_2)_6(H_2O)_3]Cl$, and Na(dbm) were prepared by published procedures.[19] All of the solvents were from BDH; THF and MeCN were distilled before use, using standard procedures.[20] For the synthesis of all of the compounds, all of the manipulations were conducted under anaerobic conditions (dinitrogen-purged glove box and argon-served Schlenk line), with the exception of **6**, which was prepared aerobically.

General Procedure for the Synthesis of $[V_2(VO)_2(acac)_4(RC\{CH_2O\}_3)_2]$ (1−3). $[V(acac)_3]$ (0.25 g, 0.72 mmol), $[VO(acac)_2]$ (0.190 g, 0.72 mmol), $RC(CH_2OH)_3$ [R = Me 0.086 g (**1**), Et 0.096 g (**2**), CH_2OH 0.098 (**3**), 0.72 mmol], and MeCN (9 mL) were

(19) (a) Manzer, L. E. *Inorg. Synth.* **1982**, *21*, 135. (b) Smith, A. Ph.D. Thesis, The University of Manchester, Manchester, U.K., 1999. (c) Halcrow, M. A.; Sun, J.-S.; Huffman, J. C.; Christou, G. *Inorg. Chem.* ***1995***, *34*, 4167.

(20) Furniss, B. S.; Hannaford, A. J.; Smith, P. W. G.; Tatchell, A. R.; *Vogel's Textbook of Practical Organic Chemistry*, 5th Ed.; Longman Scientific and Technical: Sussex, U.K., 1989.

placed in a sealed Teflon container (Parr) and heated for 12 h at 150 °C. X-ray quality crystals of the product were filtered from the cooled MeCN and dried in vacuo. $[V_2(VO)_2(acac)_4(MeC\{CH_2O\}_3)_2]$.MeCN (**1**): 58% yield. MALDI-MS (dithranol matrix, CH_2Cl_2 solution), *m/z*: 866 (molecular ion), 850 (*M* - O^{2-}), 767 (*M* - $acac^-$). Anal., observed (Calcd for $C_{32}H_{49}O_{15}NV_4$): C, 42.20 (42.35), H, 5.40 (5.44), N, 1.54 (1.54), V, 22.34 (22.45). Selected IR data (KBr), ν (cm^{-1}): 3468, 2912, 1557, 1354, 1280, 1126, 1034, 971, 784, 547. $[V_2(VO)_2(acac)_4(EtC\{CH_2O\}_3)_2]$ (**2**): 74% yield. MALDI-MS (dithranol matrix, CH_2Cl_2 solution), *m/z*: 894 (molecular ion), 878 (*M* - O^{2-}), 795 (*M* - $acac^-$). Anal., observed (Calcd for $C_{32}H_{50}O_{16}V_4$): C, 42.94 (42.97), H, 5.48 (5.63), V, 22.51 (22.78). IR (KBr), ν (cm^{-1}): 3468, 2913, 1538, 1359, 1280, 1117, 1052, 972, 545, 501. $[V_2(VO)_2(acac)_4(\{HOCH_2\}C\{CH_2O\}_3)_2]$ (**3**): 78% yield. MALDI-MS (dithranol matrix, CH_2Cl_2 solution), *m/z*: 898 (molecular ion), 882 (*M* - O^{2-}), 799 (*M* - $acac^-$). Anal., observed (Calcd for $C_{30}H_{46}O_{18}V_4$): C, 40.38 (40.11), H, 5.06 (5.16), V, 21.91 (22.68). IR (KBr), ν (cm^{-1}): 3497, 2911, 1525, 1376, 1117, 1021, 975, 934, 804, 645.

Synthesis of $[V_2(VO)_2(acac)_4(MeC\{CH_2O\}_3)_2]$ (4). The synthesis of **1** was repeated but using THF as solvent. 73% yield. MALDI-MS (dithranol matrix, CH_2Cl_2 solution), *m/z*: 866 (molecular ion), 850 (*M* - O^{2-}), 767 (*M* - $acac^-$). Anal., observed (Calcd for $C_{30}H_{46}O_{16}V_4$): C, 41.73 (41.59), H, 5.45 (5.35), V, 22.87 (23.52). IR (KBr), ν (cm^{-1}): 3468, 2912, 1557, 1354, 1280, 1126, 1033, 971, 784, 547.

Synthesis of $[V_2(VO)_2(acac)_2(O_2CPh)_2(EtC\{CH_2O\}_3)_2]$ (5). $[V(acac)_3]$ (0.25 g, 0.72 mmol), $[VO(acac)_2]$ (0.190 g, 0.72 mmol), $EtC\{CH_2OH\}_3$ (0.096 g, 0.72 mmol), $PhCO_2H$ (0.088 g, 0.72 mmol), and MeCN (9 mL) were placed in a sealed Teflon container and heated for 12 h at 200 °C. X-ray quality crystals of **5** were filtered from the cooled MeCN solution, in a 55% yield. MALDI-MS (dithranol matrix, in CH_2Cl_2 solution), *m/z*: 938 (molecular ion), 922 (*M* - O^{2-}), 817 (*M* − O_2CPh^-). Anal., observed (Calcd for $C_{36}H_{46}O_{16}V_4$): C, 46.15 (46.07), H, 4.96 (4.96), V, 21.87 (21.71). IR (KBr), ν (cm^{-1}): 3450, 2922, 1537, 1398, 1331, 1047, 982, 946, 725, 560.

Synthesis of $[(VO)_4(MeOH)_2(O_2CPh)_2(\{HOCH_2\}C\{CH_2O\}_3)_2]$. 4MeOH (6). $[V_3(O)(PhCO_2)_6(H_2O)_3]Cl$ (0.25 g, mmol), $\{HOCH_2\}C\{CH_2OH\}_3$ (0.035 g, 0.25 mmol), and MeOH (9 mL) were placed in a sealed Teflon container and heated for 12 h at 100 °C. X-ray quality crystals of **6** were formed on standing of the cooled solution for 1 d (31%). Electrospray (in MeOH solution), *m/z*: 807 (M -OMe^-). Anal., observed (Calcd for $C_{30}H_{52}O_{22}V_4$): C, 37.61 (37.20), H, 5.91 (5.41), V, 21.36 (21.04). IR (KBr), ν (cm^{-1}): 3436, 2929, 1532, 1405, 1122, 1024, 966, 723, 656, 558.

General Procedure for the Synthesis of $[V_4Cl_2(dbm)_4(RC\{CH_2OH\}_3)_2]$ (7−9). $[VCl_3(THF)_3]$ (0.2 g, 0.54 mmol), Na(dbm) (0.26 g, 1.07 mmol), $RC(CH_2OH)_3$ [R = Me 0.064 g (**7**), Et 0.072 g (**8**), CH_2OH 0.073 (**9**), 0.54 mmol], and THF (**7**, **8**) or MeCN (**9**) (9 mL) were heated in a sealed Teflon container for 12 h at 150 °C. X-ray quality crystals of product were filtered immediately from the cooled THF or MeCN solution and dried in vacuo. Filtration must be carried out immediately to avoid the precipitation of NaCl which occurs within a few minutes of opening the Teflon container. $[V_4Cl_2(dbm)_4(MeC\{CH_2O\}_3)_2]\cdot THF$ (**7**): 84% yield. Anal. (%), observed (Calcd for $C_{74}H_{70}O_{15}Cl_2V_4$): C, 60.30 (60.30), H, 4.44 (4.79), Cl, 5.00 (4.81), V, 13.63 (13.82). IR (KBr), ν (cm^{-1}): 2919, 1590, 1478, 1320, 1227, 1025, 762, 721, 686, 522. $[V_4Cl_2(dbm)_4(EtC\{CH_2O\}_3)_2]$ (**8**): 66% yield. Anal. (%), observed (Calcd for $C_{72}H_{66}O_{14}Cl_2V_4$): C, 60.39 (60.48), H, 4.57 (4.65), Cl, 5.12 (4.96), V, 14.11 (14.25). IR (KBr), ν (cm^{-1}): 294, 1589, 1527, 1337, 1227, 1041, 761, 718, 684, 523. $[V_4Cl_2(dbm)_4(\{HOCH_2\}C\{CH_2O\}_3)_2]\cdot MeCN\cdot 0.5MeOH$ (**9**): 72% yield. MALDI-MS (dithranol matrix, THF solution), *m/z*: 1433 (M^+), 1397 (*M* - Cl^-). Anal. (%), observed (Calcd for $C_{72.5}H_{67}O_{16.5}N_1Cl_2V_4$): C, 58.34 (58.40), H, 4.38 (4.54), N, 1.63 (0.94), Cl, 4.93 (4.76), V, 13.32 (13.67).

Synthesis of $[V_4Cl_2(dbm)_4(MeO)_6]$ (10). $[VCl_3(THF)_3]$ (0.2 g, 0.54 mmol), Na(dbm) (0.26 g, 1.07 mmol), and MeOH (9 mL) were heated in a sealed Teflon container for 12 h at 150 °C. X-ray quality crystals of **10** were filtered from the cooled solution and dried in vacuo. 93% yield. MALDI-MS (dithranol matrix, CH_2Cl_2 solution), *m/z*: 1317 (*M* -Cl^-). Anal. (%), observed (Calcd for $C_{66}H_{62}O_{14}Cl_2V_4$): C 58.26 (58.55), H 4.44 (4.62), Cl, 4.96 (5.24), V, 14.80 (15.08). IR (KBr), ν (cm^{-1}): 2929, 2824, 1591, 1553, 1479, 1320, 1028, 1003, 716, 537.

Table 3. Selected Structural Parameters for **1**−**4**

	1	**2**[a]	**3**[a]	**4**[a]
V(1)···V(2)	3.237	3.244	3.244	3.236
V(1)···V(2A)	3.221	3.241	3.231	3.243
V(2)···V(2A)	3.191	3.173	3.182	3.185
		$V-O_{(vanadyl)}$		
V(1)−O(8)	1.598(2)	1.6031(13)	1.601(3)	1.6304(11)
		$V-O_{(acac)}$		
V(1)−O(1)	1.992(2)	1.9818(13)	1.989(3)	1.9865(10)
V(1)−O(2)	1.993(2)	1.9875(13)	1.992(3)	1.9793(10)
V(2)−O(3)	1.979(2)	1.9708(13)	1.965(3)	1.9753(9)
V(2)−O(4)	1.973(2)	1.9717(13)	1.969(3)	1.9627(9)
		$V-O_{(tris-alkoxide)}$[a]		
V(1)−O(5)	2.008(2)	2.0154(12)	2.023(3)	2.0149(9)
V(1)−O(6A)	2.318(2)	2.3474(12)	2.338(3)	2.3367(9)
V(1)−O(7A)	2.016(2)	2.0092(12)	2.021(3)	2.0229(9)
V(2)−O(6A)	2.070(2)	2.0705(12)	2.082(3)	2.0760(9)
V(2)−O(6)	2.067(2)	2.0646(12)	2.061(3)	2.0692(9)
V(2)−O(5)	1.953(2)	1.9552(12)	1.959(3)	1.9584(9)
V(2)−O(7)	1.956(2)	1.9559(12)	1.966(3)	1.9588(9)
		$M-O_{(tris-alkoxide)}-M$		
V(1)−O(5)−V(2)	109.61(10)	109.55(6)	109.09(16)	109.06(4)
V(1)−O(7A)−V(2A)	108.39(10)	109.67(6)	108.26(15)	109.09(4)
V(1)−O(6A)−V(2A)	94.39(8)	94.34(5)	94.29(12)	94.62(3)
V(1)−O(6A)−V(2)	94.90(8)	94.27(5)	94.24(12)	94.15(3)
V(2)−O(6)−V(2A)	100.92(9)	100.24(5)	100.37(14)	100.41(4)

[a]Labeled on the basis of the atomic numbering of **1**, for simplicity.

Results and Discussion

Synthesis and Structural Studies. (i). Mixed-Valence $\{V^{III}_2V^{IV}_2\}$ Complexes. The mixed-valence $\{V^{III}_2V^{IV}_2\}$ complexes $[V_2(VO)_2(acac)_4\{RC(CH_2O)_3\}_2]$ **1**−**3** (R = Me **1**, Et **2**, CH_2OH **3**) are prepared in excellent yields (50−80%) by heating $[V(acac)_3]$, $[VO(acac)_2]$, and the appropriate $RC(CH_2OH)_3$ triol (1:1:1) in MeCN at 150 °C for 12 h, followed by slow cooling to give crystalline products directly from the reaction solutions. The same products are also isolated, but in much lower yields (<10%), if $[VO(acac)_2]$ is omitted from the reactions. **1** crystallizes with a single molecule of MeCN as solvate − if the reaction is carried out in THF **1** crystallizes without solvate (**4**). Selected structural parameters for **1**−**4** are given in Table 3; these have identical connectivites other than the R group of the tris-alkoxide ligands, and only **1** will be described in detail here.

Molecules of **1** (Figure 1) lie on a crystallographic inversion center; the four vanadium ions are coplanar, occupying the corners of a rhombus. V(2)···V(2A) defines the short diagonal. V(1) and symmetry equivalent (s.e.) have a terminal oxide O(8) at 1.598(2) Å, characteristic of vanadyl,

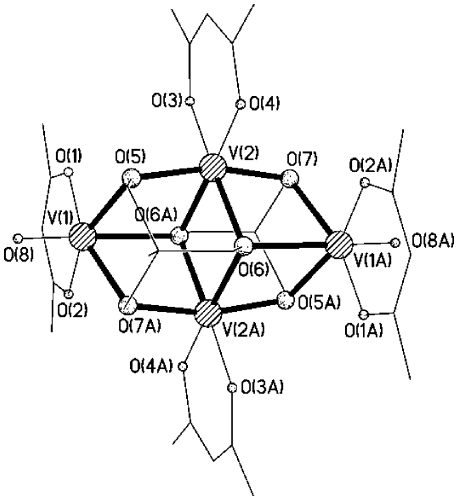

Figure 1. Structure of $[V_2(VO)_2(acac)_2(MeC\{CH_2O\}_3)_2]$ (**1**). Scheme: Striped lines (vanadium), dotted (oxygen), vertex (carbon); hydrogen atoms omitted for clarity.

whereas V(2) is V^{III} as assigned by bond valence sum (BVS) calculations,[21] and is consistent with its regular octahedral geometry and with charge-balance requirements. The four metal ions are bound by two triply deprotonated, μ_2,μ_2,μ_3-$(MeC\{CH_2O\}_3)^{3-}$ ligands. Each μ_2 arm of the tris-alkoxides [O(5), O(7) and s.e.] bridges an edge of the rhombus. The μ_3 arms of the two tris-alkoxides bridge V(1), V(2), and V(2A) (and s.e.), forming a butterfly core, where the V^{III} ions define the body and the V^{IV} ions define the wingtips (*type A*, Scheme 1). A chelating diketonate completes the six-coordination at each metal ion.

The structures of **1**−**4** are closely related to the only other tetrametallic mixed-valence $V^{III/IV}$ cluster, Mikuriya's $[V_2(VO)_2(acac)_4(OMe)_6]$,[5] where six methoxides take the place of the two $(MeC\{CH_2O\}_3)^{3-}$ in **1**−**4**.

Addition of a carboxylic acid to the reaction that gives **1**−**4** − for example, reaction of $[V(acac)_3]$, $[VO(acac)_2]$, $EtC\{CH_2OH\}_3$, and $PhCO_2H$ (1:1:1:1) in MeCN at 200 °C for 12 h − gives $[V_2(VO)_2(PhCO_2)_2(EtC\{CH_2O\}_3)_2]$ (**5**) in good yield. **5** is also centrosymmetic and has a mixed-valence $\{V^{III}_2V^{IV}_2\}$, butterfly metal-alkoxo core (Figure 2 and Table 4). In contrast to **1**−**4**, where the butterfly body is defined by $V^{III}\cdots V^{III}$, in **5**, the body is $V^{IV}\cdots V^{IV}$ (*type B*, Scheme 1), and this has important consequences for the magnetic behavior (later in this article). The V^{IV} ions V(2) and s.e. are bridged by the μ_3-O(6,6A) arms of the triols. O(6) is trans to the terminal oxide O(8A) at V(2A), such that the $[(VO)_2\{\mu\text{-}O(R)\}_2]$ butterfly body is planar, with an anti-coplanar configuration in Plass' classification of such divanadyl fragments.[8] V1 and s.e. have chelating diketonates and two μ_2-benzoates bridge these metal ions to V(2A) and s.e., respectively.

(ii). Homovalent $\{V^{IV}_4\}$ Complexes. The homovalent tetravanadyl cluster $[(VO)_4(MeOH)_2(O_2CPh)_2(\{HOCH_2\}C\{CH_2O\}_3)_2]$ (**6**) can be prepared in ca. 30% yield by the reaction of the basic metal carboxylate $[V_3(O)(PhCO_2)_6(H_2O)_3]Cl$ with $C\{CH_2OH\}_4$ in MeOH at 100 °C. This reaction is conducted under aerobic conditions, allowing the oxidation of the V^{III} starting material. **6** is centrosymmetric and crystallizes with four molecules of methanol (Figure 2 and Table 4). All of the vanadium ions are present as vanadyl, but the oxometallic core is otherwise similar to **1**−**5**, bound by two triply deprotonated $(\{HOCH_2\}C\{CH_2O\}_3)^{3-}$ ligands [the fourth alcohol, O(9), remains protonated]. Benzoates provide an additional bridge between V(1) and V(2A), as observed in **5**, and methanol completes the coordination spheres of V(1) and s.e. The $\{V^{IV}_4\}$ butterfly body is V(2)···V(2A) with an anti-coplanar[8] $[(VO)_2\{O(R)\}_2]$ configuration (as in **5**). The body−wingtip fragments are also of the form $[(VO)_2\{O(R)\}_2]$, and the relationships between the vanadyls are syn-coplanar [V(2)···V(1A) and s.e.] and twist [V(2)···V(1) and s.e.] in Plass' classification.[8] The same tetra-vanadyl topology has been observed in $[(VO)_4L_2(acac)_2(OMe)_2]$.[15]

(iii). Homovalent $\{V^{III}_4\}$ Complexes. The homovalent $\{V^{III}_4\}$ clusters $[V_4Cl_2(dbm)_4(RC\{CH_2O\}_3)_2]$ [R = Me **7**, Et **8** or $HOCH_2$ **9**] can be isolated from the solvothermal reaction of $[VCl_3(THF)_3]$ with triol and Na(dbm) (Hdbm = dibenzoylmethane) in THF or MeCN under anaerobic conditions. $[VCl_3(THF)_3]$ and Na(dbm) were dissolved to give a dark-brown solution, possibly indicating the formation of $[V(dbm)_3]$. The triol was added, and the system was heated at 150 °C for 12 h and then cooled to give red crystals of $[V_4Cl_2(dbm)_4(RC\{CH_2O\}_3)_2]$ (Figure 3). **7** crystallizes with a molecule of THF and **9** crystallizes with MeCN and MeOH. Similar reactions but *without* the triol and in MeOH as solvent yield $[V_4Cl_2(dbm)_4(OMe)_6]$ (**10**, Figure 3) in over 90% yield.

7−**10** have cores analogous to **1**−**6**, but contain only V^{III} ions as, indicated by BVS calculations[21] and charge balance. Each metal has a chelating dbm^-, and V(1) and s.e. have a terminal chloride. **7** is identical to **1** except for the replacement of the two $\{V^{IV}{=}O\}^{2+}$ vanadyl units of **1** with two isoelectronic $\{V^{III}{-}Cl\}^{2+}$ moieties [V−Cl 2.3325(18) Å]. In **10**, the six methoxides replace the six arms of the two tris-alkoxides of **8** and **9**. The $\{V^{III}_4\}$ butterfly bodies have $V^{III}{-}\mu_3O{-}V^{III}$ angles of ca. 100° (Table 5), very similar to the corresponding *type A* $\{V^{III}_2V^{IV}_2\}$ cores (Scheme 1) of **1**−**4**.

Magnetic Studies. The magnetic properties of all of the *type A* $\{V^{III}_2V^{IV}_2\}$ complexes **1**−**3** are similar (Supporting Information), and only those for **3** will be presented here. The room-temperature value of χT (χ = molar magnetic susceptibility, T = temperature) is 2.62 emu K mol^{-1}, in good agreement with that expected for two V^{III} and two V^{IV} uncoupled spins. χT decreases with decreasing T (Figure 4, top), indicative of dominant antiferromagnetic exchange interactions within the cluster.

Given the crystallographic C_i point symmetry of the molecule (Scheme 1), and assuming the wingtip−wingtip interactions to be nil, we have the exchange spin Hamiltonian:

$$H = -J_{wb1}[\hat{S}_{V1}\hat{S}_{V2} + \hat{S}_{V1A}\hat{S}_{V2A}] - J_{wb2}[\hat{S}_{V1}\hat{S}_{V2A} + \hat{S}_{V1A}\hat{S}_{V2}] - J_{bb}\hat{S}_{V2}\hat{S}_{V2A}$$

(21) Liu, W.; Thorp, H. H. *Inorg. Chem.* **1993**, *32*, 4102.

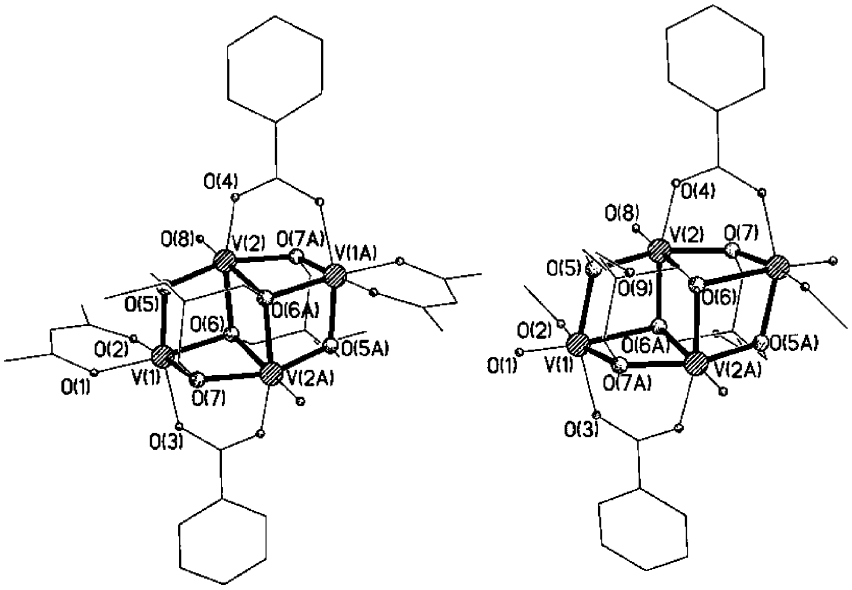

Figure 2. Structures of $[V_2(VO)_2(PhCO_2)_2(EtC\{CH_2O\}_3)_2(acac)_2]$ (**5**, left) and $[(VO)_4(MeOH)_2(O_2CPh)_2(\{HOCH_2\}C\{CH_2O\}_3)_2]$ (**6**, right).

Table 4. Selected Structural Parameters for **5** and **6**

5		**6**		**6′**[a]
V(1)−V(2)	3.0515(7)	V(1)−V(2)	3.218	3.183
V(1)−V(2A)	3.127	V(1)−V(2A)	3.188	3.197
V(2)−V(2A)	3.525	V(2)−V(2A)	3.394	3.411
$V-O_{(vanadyl)}$		$V-O_{(vanadyl)}$		
		V(1)−O(1)	1.587(3)	1.590(3)
V(2)−O(8)	1.5984(19)	V(2)−O(8)	1.614(3)	1.605(3)
$V-O_{(acac)}$		$V-O_{MeOH)}$		
V(1)−O(1)	1.9676(19)			
V(1)−O(2)	1.9470(19)	V(1)−O(2)	2.032(3)	2.043(3)
$V-O_{(benzoate)}$		$V-O_{(benzoate)}$		
V(1)−O(3)	2.024(2)	V(1)−O(3)	2.022(3)	2.035(3)
V(2)−O(4)	2.030(2)	V(2)−O(4)	2.033(3)	2.015(3)
$V-O_{(tris-alkoxide)}$		$V-O_{(tris-alkoxide)}$		
V(1)−O(5)	1.960(2)	V(1)−O(5)	2.004(3)	2.005(3)
V(1)−O(6)	2.0596(18)	V(1)−O(6A)	2.258(3)	2.240(3)
V(1)−O(7)	1.9906(19)	V(1)−O(7A)	1.976(3)	1.973(3)
V(2)−O(6)	2.009(2)	V(2)−O(6A)	1.988(3)	2.307(3)
V(2)−O(6A)	2.4138(19)	V(2)−O(6)	2.296(3)	1.986(3)
V(2)−O(5)	1.9946(18)	V(2)−O(5)	1.985(3)	1.994(3)
V(2)−O(7A)	1.9694(18)	V(2)−O(7)	1.972(3)	1.971(3)
$M-O_{(tris-alkoxide)}-M$		$M-O_{(tris-alkoxide)}-M$		
V(1)−O(5)−V(2)	101.01(9)	V(1)−O(5)−V(2)	107.57(13)	106.16(13)
V(1)−O(7)−V(2A)	104.30(9)	V(1)−O(7A)−V(2A)	107.72(13)	107.66(13)
V(1)−O(6)−V(2A)	88.32(7)	V(1)−O(6A)−V(2A)	88.86(10)	88.87(10)
V(1)−O(6)−V(2)	97.16(9)	V(1)−O(6A)−V(2)	98.34(12)	98.17(11)
V(2)−O(6)−V(2A)	105.30(8)	V(2)−O(6)−V(2A)	104.56(12)	104.97(12)

[a] Two half molecules in the asymmetric unit (**6** and **6′**).

where $J_{wb1,2}$ are the body−wingtip interactions ($V^{III}...V^{IV}$), and J_{bb} is the body−body interaction between the two V^{III} ions. We initially attempted to fit the data with only two unique J values, that is, with $J_{wb1} = J_{wb2}$. This simplified model failed to give a satisfactory fit; hence, we allowed J_{wb1} and J_{wb2} to differ. This gave a best fit (Figure 4, top) with $J_{wb1} = -9.9 \pm 0.5$, $J_{wb2} = -8.8 \pm 1$, and $J_{bb} = -16.3 \pm 1$ cm^{-1} (all antiferromagnetic), with $g = 2.02 \pm 0.0.2$. Note that J_{wb1} and J_{wb2} can be interchanged in this Hamiltonian, that is, this model does not unambiguously assign which interaction is V(1)···V(2) and which is V(1)···V(2A). Mikuriya et al. reported values equivalent to $J_{wb1} = J_{wb2} = 0$, and $J_{bb} = -82.6$ cm^{-1} (values converted to be consistent with our Hamiltonian, J_{wb1} and J_{wb2} were constrained to be equal) for $[V_2(VO)_2(acac)_4(OMe)_6]$, which also has a *type A* butterfly core;[5] however, their magnetic data was only measured down to 80 K, so these values should be treated with some caution.

The shape of a low-temperature (1.6 K) molar magnetization (M) versus an applied magnetic field (B) curve is consistent with an $S = 0$ ground state, crossing with a low-lying $S = 1$ excited state (point of inflection at ca. 3 T), saturating at 2 μ_B (Figure 4, bottom). The J values above would give a singlet ground state with lowest excited states

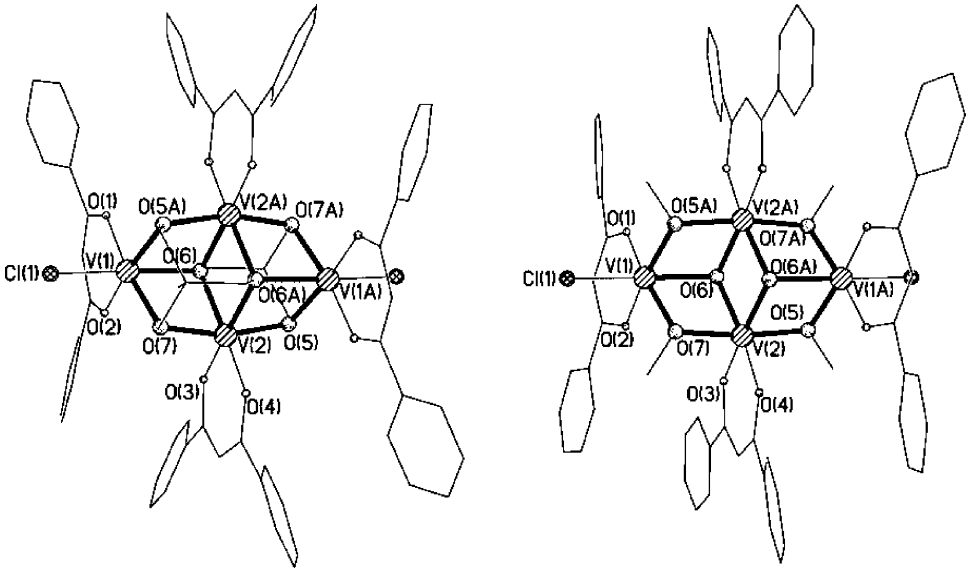

Figure 3. Views of $[V_4Cl_2(dbm)_4(MeC\{CH_2O\}_3)_2]$ (**7**, left) and $[V_4Cl_2(dbm)_4(OMe)_6]$ (**10**, right).

Table 5. Selected Structural Parameters for **7**−**10**

	7	**8**	**8′**[a]	**9**	**10**
V(1)−V(2)	3.140	3.139	3.124	3.0930(6)	3.1171(6)
V(1)−V(2A)	3.120	3.1177(6)	3.131	3.136	3.126
V(2)−V(2A)	3.224	3.222	3.225	3.221	3.161
		V−Cl			
V(1)−Cl(1)	2.3325(18)	2.3142(8)	2.2691(10)	2.3529(7)	2.3383(7)
		$V-O_{(dbm)}$			
V(1)−O(1)	1.952(4)	1.9489(17)	1.958(2)	1.9344(17)	1.9521(14)
V(1)−O(2)	1.955(4)	1.9680(17)	1.9564(19)	1.9438(16)	1.9549(14)
V(2)−O(3)	1.941(4)	1.9486(16)	1.9578(19)	1.9396(16)	1.9694(14)
V(2)−O(4)	1.945(4)	1.9460(17)	1.9544(18)	1.9463(17)	1.9586(13)
		$V-O_{(tris-alkoxide)}$[a]			
V(1)−O(5A)	1.995(4)	2.0105(17)	1.9948(19)	1.9927(16)	1.9762(13)
V(1)−O(6)	2.144(4)	2.1368(16)	2.1405(19)	2.1319(16)	2.1379(13)
V(1)−O(7)	2.009(4)	1.9847(16)	2.0065(19)	1.9547(16)	1.9708(13)
V(2)−O(6)	2.112(3)	2.0888(16)	2.0905(18)	2.0972(16)	2.0493(13)
V(2)−O(6A)	2.106(3)	2.0976(16)	2.0896(18)	2.0991(16)	2.0738(13)
V(2)−O(5)	1.950(4)	1.9442(17)	1.957(2)	1.9539(16)	1.9606(13)
V(2)−O(7)	1.948(4)	1.9580(17)	1.943(2)	1.9547(16)	1.9791(13)
		$M-O_{(tris-alkoxide)}-M$			
V(1)−O(5A)−V(2A)	104.54(17)	105.08(7)	104.82(9)	105.22(7)	105.15(6)
V(1)−O(7)−V(2)	105.00(16)	104.50(7)	104.54(9)	103.47(7)	104.22(6)
V(1)−O(6)−V(2)	95.10(14)	95.08(6)	95.16(7)	94.00(6)	96.20(5)
V(1)−O(6)−V(2A)	94.74(14)	95.70(6)	95.50(7)	95.65(6)	95.85(5)
V(2)−O(6)−V(2A)	99.71(14)	100.64(7)	100.99(8)	100.28(6)	100.09(5)

[a] Two half molecules in the asymmetric unit (**8** and **8′**).

at 3.4 ($S = 1$), 3.8 ($S = 0$), and 10.1 cm^{-1} ($S = 1$), and we can simulate the *M* versus *B* curve using only these four states, with the inclusion of a ZFS of $|D| = 0.35$ cm^{-1} in the lower triplet (the curve is practically insensitive to the sign of this *D* and to the ZFS of the upper triplet). The low-temperature (<10 K) χT versus *T* data can also be reproduced using only these states (Figure 4 top, insert). This value of $|D|$ is consistent with the low-temperature W-band EPR spectrum (Figure 5), which shows a clearly defined spin triplet state. Note that at the $g \approx 2$ resonance fields for W band the lowest triplet is now the ground state.

The magnetic behavior of the *type B* $\{V^{III}_2V^{IV}_2\}$ complexes are very different: for **5**, χT is 2.09 emu K mol^{-1} at room temperature and decreases steadily with decreasing temperature (Figure 6), indicating considerably stronger antiferromagnetic coupling than observed for the *type A* complexes. χT plateaus at ca. 0.89 emu K mol^{-1} between ca. 50−10 K, below which it decreases slightly. *M* versus *B* data are tending toward saturation at ca. 2 μ_B. All of these data are consistent with a well-isolated $S = 1$ ground state. Fitting χT using the same model as used for **3** (Scheme 2), gives $J_{wb1} = -105 \pm 3$ cm^{-1}, $J_{wb2} = -27.8 \pm 5$ cm^{-1} with J_{bb} set to $+5.0$ cm^{-1} (*g* fixed at 1.95; Figure 6), where the J_{bb} interaction is now between the two vanadyl ions. The fit is insensitive to J_{bb} because of the large magnitude of J_{wb1} (later in this article). However, J_{bb} is expected to be weakly

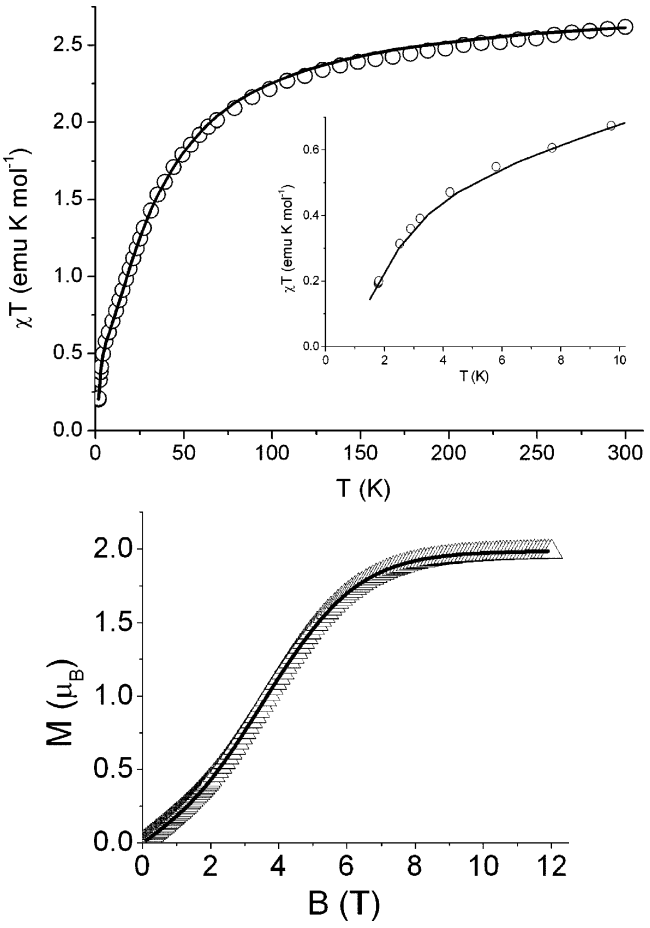

Figure 4. Top: χT versus T for **3** and best fit using the J values in the text (solid line). Inset: Low-temperature χT versus T data and calculated curve including only the bottom four total spin states (solid line). Bottom: M versus B at 1.6 K and simulation (solid line) using the same model as the inset.

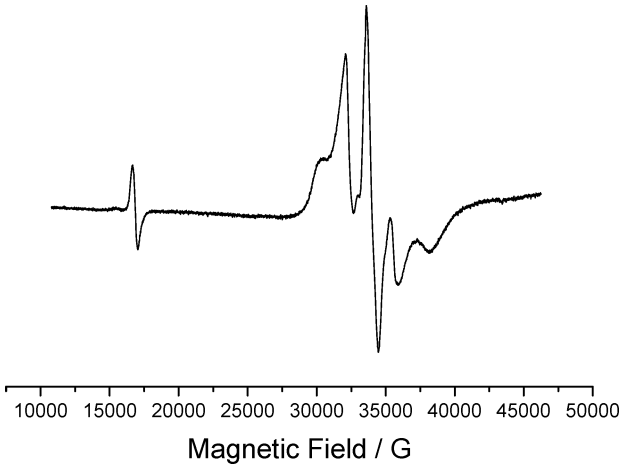

Figure 5. W-band (94.01 GHz) EPR spectrum of a polycrystalline sample of **3** at 5 K.

ferromagnetic because the anti-coplanar configuration of the two vanadyl ions leads to accidental orthogonality of the magnetic orbitals (Scheme 2, right).[8] Hence, we have fixed $J_{bb} = +5.0$ cm^{-1}, consistent with structurally related vanadyl dimers.[8,22] These J values give a triplet ground state with

(22) Tsaramyrsi, M.; Kaliva, M.; Salifoglou, A. *Inorg. Chem.* **2001**, *40*, 5772.

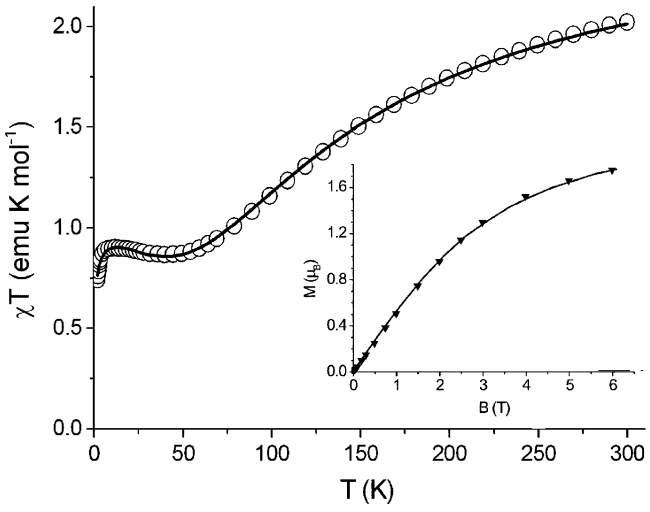

Figure 6. χT versus T for **5** and best fit (solid line) with the parameters in the text. Inset: M versus B at 2 K and best fit (solid line) considering only the ground state.

Scheme 2. Relationship of the Vanadyl $\{V^{IV}{=}O\}^{2+}$ to V^{III} Ions in the *Type A* and *Type B* $\{V^{III}_2V^{IV}_2\}$ Cores of, for Example, **3** and **5**, Respectively[a]

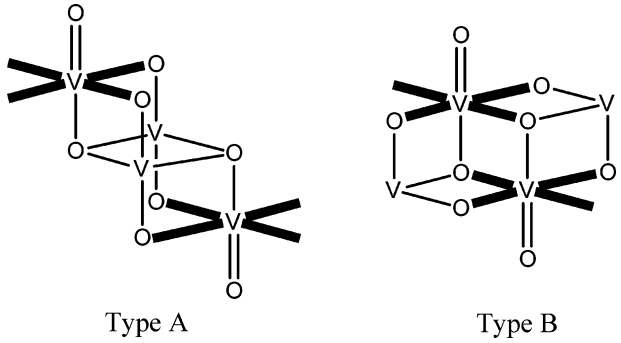

[a] The vanadium ions without terminal oxides are V^{III}. The equatorial bonds of the d^1 vanadyl ions are emboldened to emphasize their local *xy* planes, where the local *z* axes are defined by V═O, and; hence, the planes of their magnetic d_{xy} orbitals. The two $V^{IV}\cdots V^{III}$ interactions are equivalent in *Type A* but different in *Type B*.

first excited states at 30.1 cm^{-1} ($S = 0$) and 157 cm^{-1} ($S = 2$ and 1). An intermolecular interaction term is included in the fit to account for the slight decrease in χT below 10 K.[23]

In contrast to **3**, we *can* assign J_{wb1} and J_{wb2} in **5** on structural arguments. The single unpaired electron in the vanadyl ions is expected to reside in the $3d_{xy}$ orbital, where *z* is defined by V═O, on the basis of simple crystal-field theory arguments. Considering either vanadyl ion in the *type B* core, one of the V^{III} ions lies in the local *xy* plane, whereas the other lies out of the plane (Scheme 2, right). Hence, we expect a much-stronger $V^{III}\cdots V^{IV}$ interaction for the former than the latter. Thus, $J_{wb1} = -105$ cm^{-1} must be the V(1)···V(2) (and s.e.) interaction, whereas $J_{wb2} = -28$ cm^{-1} is V(1)···V(2A) and s.e. In contrast, these two interactions are

(23) The intermolecular term is included as $\chi_f = \chi_c(1 - \theta\chi_c)^{-1}$, where χ_c is the susceptibility calculated in the absence of intermolecular interactions and χ_f is the final fitting value. The value of θ is related to the intermolecular exchange constant J' by: $\theta = zJ'/(g^2N_i\mu_B^2) = zJ'/(g^20.2607)$, where *z* is the number of nearest neighboring molecules, giving $J' = 0.53$ cm^{-1}. The approximation is reliable only when θ (and J') are not too large with respect to the other coupling constants in the systems, see O'Connor, C. J. *Prog. Inorg. Chem.* **1982**, *29*, 203.

chemically equivalent in *type A* cores (Scheme 2, left), consistent with the numerically similar and small values of J_{wb1} and J_{wb2} (ca. -9 cm^{-1}) found for **3** (above). The 2 K M versus B curve for **5** can be simulated successfully (Figure 6, inset), considering only the $S = 1$ ground state (consistent with the first excited state being at 30 cm^{-1}) with $g = 1.93 \pm 0.03$ and an axial ZFS of $|D| = 2.5 \pm 0.3$ cm^{-1} ($H = \mu_B g \hat{S}\,\mathbf{B} + D\hat{S}_z^2$).

In summary, the *type A* and *type B* $\{V^{III}_2V^{IV}_2\}$ cores give rise to very different magnetic behavior − the former leads to an $S = 0$ ground state with a number of low-lying excited states, whereas the latter leads to a well-isolated $S = 1$ ground state.

For the *type A* systems, all of the magnetic interactions are antiferromagnetic and cannot be satisfied simultaneously − for example, if we assign the two V^{III} spins to be antiparallel in the lowest energy configuration ($|J_{bb}|$ being the strongest interaction), then the two J_{wb} interactions are competing to align the V^{IV} spins. A number of states of similar energy arise because the competing antiferromagnetic J_{wb1}, J_{wb2}, and J_{bb} are similar in magnitude to each other, with the ground state depending on the J_{wb}/J_{bb} ratio(s)[3] (we avoid the term "spin frustration" because this applies strictly to systems with degenerate ground states).[24] Useful insight into the nature of the lowest-lying states is possible through a simple Kambé analysis. We define the butterfly body ($S = 1$) and wingtip ($S = {}^1/_2$) spins as $S_{1,2}$ and $S_{3,4}$, respectively, the intermediate spin operators $\hat{S}_A = \hat{S}_1 + \hat{S}_2$ and $\hat{S}_B = \hat{S}_3 + \hat{S}_4$, and the total-cluster spin operator $\hat{S} = \hat{S}_A + \hat{S}_B$. The energies of the total cluster spin states, defined by (S, S_A, S_B), are given by (Supporting Information for full details; we have approximated $J_{wb1} = J_{wb2}$ ($= J_{wb}$) for simplicity]:

$$E = -J_{bb}[S_A(S_A + 1) - 4] - J_{wb}[S(S + 1) - S_A(S_A + 1) - S_B(S_B + 1)]$$

The relative energies for all possible spin states (S, S_A, S_B) are given in the Supporting Information and are plotted as a function of J_{wb}/J_{bb} in Figure 7. For $J_{wb}/J_{bb} < 0.5$, the degenerate pair of (0,0,0) and (1,0,1) states are lowest in energy; for $0.5 < J_{wb}/J_{bb} < 2.0$, the (0,1,1) state is lowest; for $J_{wb}/J_{bb} > 2.0$, the (1,2,1) state is lowest. The experimental value of J_{wb}/J_{bb} of 0.57 (averaging J_{wb1} and J_{wb2}) gives the (0,1,1) ground state. Note this is not the singlet state that might be expected by simply pairing the V^{III} spins and the V^{IV} spins; this (0,0,0) state is the first excited state at a relative energy of $J_{bb} - 2J_{wb}$. The lowest-lying paramagnetic states are the (1,0,1) and (1,1,1) triplets at $J_{bb} - 2J_{wb}$ and $-J_{wb}$, respectively, above the ground state.

The (1,0,1) triplet arises from coupling the two V^{III} ions to give $S_A = 0$, and the two V^{IV} ions to give $S_B = 1$. The ZFS for this state is expected to be small, arising solely from dipolar and anisotropic exchange, because the single-ion ZFS of the V^{III} ions will not make any contribution (obviously there is no single-ion ZFS for the V^{IV} ions). The small,

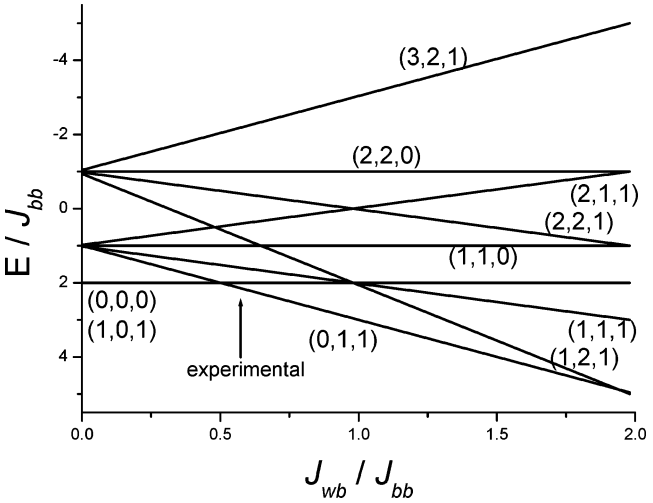

Figure 7. Relative energies E of the total spin states (S, S_A, S_B) as a function of the J_{wb}/J_{bb} ratio for an idealized *type A* $\{V^{III}_2V^{IV}_2\}$ butterfly core.

measured ZFS of $|D| = 0.35$ cm^{-1} is consistent with this being similar to that found in, for example dimeric copper acetate.[25]

For the *type B* systems, the well-isolated $S = 1$ ground state is consistent with a simple spin structure of the two V^{III} ions "spin up" and the V^{IV} ions "spin down". This simultaneously satisfies the (predicted) ferromagnetic $V^{III}\cdots V^{III}$ and antiferromagnetic $V^{III}\cdots V^{IV}$ interactions. This is the (1,1,2) state, where S_A is now the result of coupling the two V^{IV} ions, and S_B the result of two V^{III} ions. Applying a similar Kambé analysis and assuming a large antiferromagnetic J_{wb} gives the first excited state as the (0,1,1) singlet at J_{wb} above (1,1,2) over a huge range of J_{bb}/J_{wb} (Supporting Information). In **5**, J_{wb1} and J_{wb2} are very different, but this qualitative result remains valid and is consistent with the ground-state first-excited-state gap of 30 cm^{-1} (being largely determined by the smaller of J_{wb1} and J_{wb2}) from matrix diagonalization methods (above). This also illustrates that the value of J_{bb} is essentially indeterminate. Using a simple vector-coupling approach,[26] and assuming negligible anisotropic exchange contributions and collinearity of the V^{III} ZFS tensors, the (1,1,2) ground-state ZFS would be given by $D = +0.7D_{SI}$, where D_{SI} is the single-ion ZFS of V^{III}. The large ground state $|D| = 2.5$ cm^{-1}, obtained from modeling M versus B (above), is consistent with this, giving $|D_{SI}| = 3.6$ cm^{-1}, which is of the expected magnitude for V^{III}.[2]

For the homovalent $\{V^{IV}_4\}$ system **6**, χT has a room-temperature value of 1.24 emu K mol^{-1}, consistent with four uncoupled V^{IV} ions with $g < 2.0$, dropping to 0.07 emu K mol^{-1} at 2 K (Figure 8, bottom), indicative of dominant antiferromagnetic interactions, leading to a singlet ground state.

The core of **6** is equivalent to Plass' $[(VO)_4L_2(acac)_2(OMe)_2]$.[15] In his classification, this consists of an anti-coplanar [V(2)···V(2A)], two twist [V(1)···V(2) and s.e.], and two syn-coplanar [V(1)····V(2A) and s.e.] vanadyl···

(24) Kahn, O. *Chem. Phys. Lett.* **1997**, *265*, 109.

(25) Bleaney, B.; Bowers *Proc. R. Soc. London* **1952**, 451.

(26) Bencini, A.; Gatteschi, D. *EPR of Exchange Coupled Systems*, Springer-Verlag: Berlin, 1990.

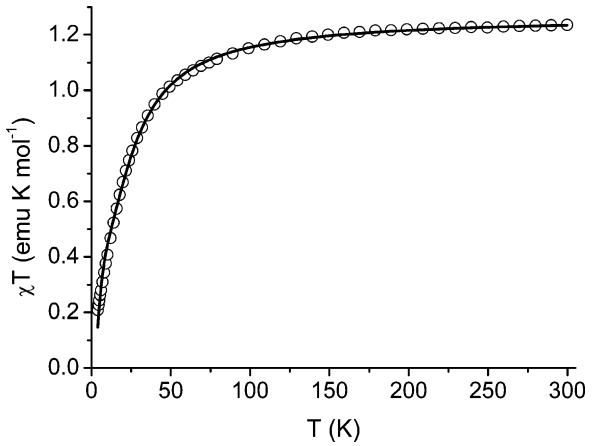

Figure 8. χT versus T for **6** and best fit (solid line) using the parameters in the text.

vanadyl interactions (Figure 2, right). As noted above, the anti-coplanar interaction (corresponding to J_{bb}) is expected to be weakly ferromagnetic, as are the twist interactions (J_{wb1}),[15] whereas the syn-coplanar interactions (J_{wb2}) are expected to be strongly antiferromagnetic from simple orbital-overlap arguments.[8] In $[(VO)_4L_2(acac)_2(OMe)_2]$, the syn-coplanar interaction (-153 cm^{-1}) dominates, giving a singlet ground state, with the calculated susceptibility behavior insensitive to the other interactions in the range $+1 \pm 50$ cm^{-1}.[15] Fitting χT for **6**, using the same model as **3** (Scheme 2) where all of the metal ions are now V^{IV}, gives $J_{wb1} = +9.0 \pm 3$, $J_{wb2} = -14.8 \pm 3$, and $J_{bb} = -32.7 \pm 1$ cm^{-1}, with g fixed at 1.84 (Figure 8). We have assigned the two wing−body interactions on the basis of their expected signs. These values are significantly different from Plass' tetramer. J_{bb} is moderately *anti*ferromagnetic but within Plass' uncertainties. More significantly, J_{wb2} is only *weakly* antiferromagnetic (in fact it is the much-smaller value of J_{wb2} in our compound that makes the fits sensitive to J_{wb1} and J_{bb}). We stress that no other combination of coupling constants reproduced the experimental curve. A possible reason for this unexpected behavior is the smaller V−O−V angles, corresponding to the (syn-coplanar) J_{wb2} interactions in **6** (107.7 and 88.9°), rather than in Plass' complex (116.7 and 96.7°).

Homovalent $\{V^{III}_4\}$ **8** has a room-temperature χT value of 3.02 emu K mol^{-1}, which is already decreasing with decreasing T, reaching 0.04 emu K mol^{-1} at 2 K (Figure S7 in the Supporting Information). The data can be fitted using the same model as **3**, where all of the metal ions are now V^{III}, giving $J_{wb1} = J_{wb2} = -26.0 \pm 5$, and $J_{bb} = -22.3 \pm 5$ cm^{-1}, with g fixed at 1.94 (Figure 9). The fit requires the inclusion of a 5% paramagnetic impurity, to account for the increase in χ versus T at very low temperature (Figure 9). Note that even allowing J_{wb1} and J_{wb2} to fit as independent parameters gives $J_{wb1} = J_{wb2}$ to three significant figures. **10** exhibits similar behavior. The $V^{III}\cdots V^{III}$ exchange observed in the butterfly body in **8**, $J_{bb} = -22$ cm^{-1}, is similar to that observed in the equivalent $V^{III}\cdots V^{III}$ unit of **3** ($J_{bb} = -16$ cm^{-1}), consistent with the similar $V^{III}-O-V^{III}$ angles. These values are also consistent with values reported for dimeric V^{III} systems with similar bridging angles.[12]

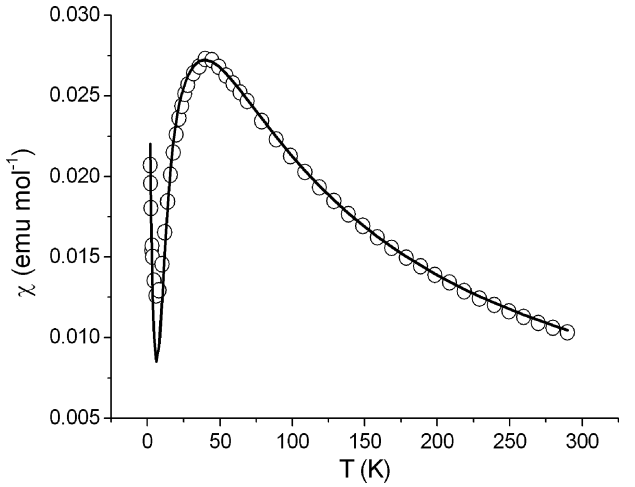

Figure 9. χ versus T for **8** and best fit (solid line) using the parameters in the text.

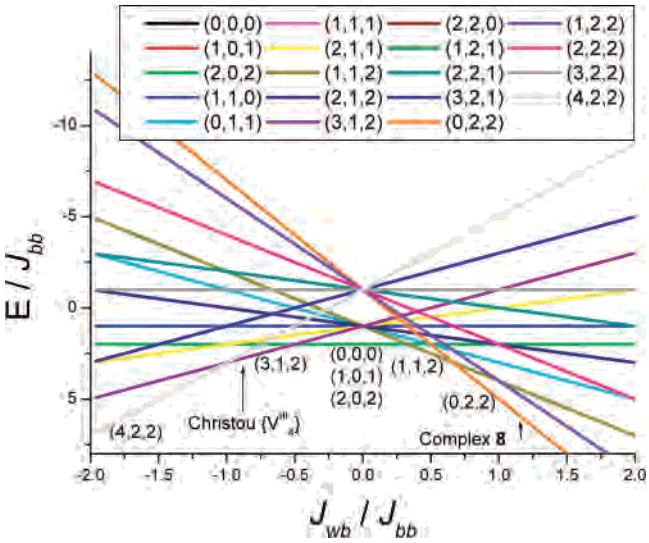

Figure 10. Relative energies E of the total spin states (S, S_A, S_B) as a function of the J_{wb}/J_{bb} ratio for an idealized $\{V^{III}_4\}$ butterfly core, with possible ground states highlighted and the two known examples marked.

Hendrickson and Christou have treated a $\{V^{III}_4\}$ butterfly arrangement by Kambé methods[3] − in their oxo-bridged $[V_4O_2(O_2CR)_7(bipy)_2]^+$ cluster there are competing antiferro- (J_{bb}) and ferro- (J_{wb}) magnetic interactions, which stabilize the (3,1,2) state with a low-lying (4,2,2) excited state. They considered possible ground states for J_{wb} and J_{bb} of opposite signs; we have extended this analysis to allow for J_{wb} and J_{bb} having the same sign, as is the case in **8** (Figure 10). Thus, the competing antiferromagnetic J values in **8** lead to the singlet (0,2,2) ground state, corresponding to the simple "spin up−spin down" arrangement around the metal rhombus, with the first excited state at a relative energy of $|J_{wb}|$. Figure 10 shows that (0,2,2) is the ground state for $J_{wb}/J_{bb} >$ ca. 0.65.

Conclusions

In conclusion, we have prepared a family of clusters based on alkoxide-bridged butterfly cores with oxidation states $\{V^{IV}_4\}$, $\{V^{III}_2V^{IV}_2\}$ (both isomeric forms), and $\{V^{III}_4\}$. These form a unique redox family of cluster species, further

extended by known[13] diamagnetic $\{V^{V}_4\}$ analogues. The $\{V^{III}_2V^{IV}_2\}$ and $\{V^{III}_4\}$ species are rare examples of heterovalent $V^{III/IV}$ and homovalent V^{III} clusters. These have all been prepared in good yield and from simple starting materials, via solvothermal synthesis. This highlights the utility of these methods in the isolation of low-valent vanadium clusters[6,7] – analogous reactions at room temperature or under reflux give only powders from which no clean products could be isolated. Magnetic studies have allowed the magnetic exchange interactions to be determined (unless these parameters are inherently indeterminate). Hence, we have developed a detailed picture of the electronic structures of these low-valent vanadium species and how these change on systematic changes in (i) the metal ion oxidation states and therefore electron count, and (ii) the geometric arrangement of the metal ions, for example between *type A* and *type B* $\{V^{III}_2V^{IV}_2\}$ cores, without gross changes in the metal-alkoxo core. It is our hope that this will aid in the understanding of the magnetic properties of high-nuclearity low-valent vanadium systems, particularly given that the $\{M_4(\mu_3\text{-}O)_2\}$ fragment is a common building block in larger clusters.

Acknowledgment. We thank the EPSRC, the Ramsey Memorial Trust (RHL), and the EC (NMP3-CT-2005-515767 "Magmanet") for funding.

Supporting Information Available: Crystallographic cif files and thermal ellipsoid plots for **1**−**10** and details of Kambé analyses. This material is available free of charge via the Internet at http://pubs.acs.org.

IC7011183